

## ORIGINAL ARTICLE

Special Section: Tribute to Rien van Genuchten, Recipient of the 2023 Wolf Prize for Agriculture

# Effects of dynamic capillarity on the shear strength of sandy soils during transient two-phase flow: Insights from non-equilibrium triaxial simulations

Alireza Daman Shokouh<sup>1</sup>  | Ehsan Nikooee<sup>1</sup>  | Ghassem Habibagahi<sup>1</sup> | S. Majid Hassanizadeh<sup>2,3</sup>

<sup>1</sup>Department of Civil and Environmental Engineering, School of Engineering, Shiraz University, Shiraz, Iran

<sup>2</sup>Stuttgart Center for Simulation Science (SIMTECH), Integrated Research Training Group, SFB 1313, Stuttgart University, Stuttgart, Germany

<sup>3</sup>Department of Earth Sciences, Utrecht University, Utrecht, The Netherlands

## Correspondence

Ehsan Nikooee, Department of Civil and Environmental Engineering, School of Engineering, Shiraz University, P.O. Box 71348-51156, Shiraz, Iran.

Email: [enikooee@shirazu.ac.ir](mailto:enikooee@shirazu.ac.ir)

Assigned to Associate Editor Jirka Simunek.

## Funding information

Stuttgart Center for Simulation Science (SimTech)

## Abstract

Modeling two-phase flow in unsaturated porous media is not only important to vadose zone hydrology but also of great value in diverse disciplines. Common approaches use a simplified relationship between fluid pressure difference and saturation, neglecting the influence of saturation change rates. However, many studies have suggested that the applicability of this approach is limited to situations where the rate of change in saturation is insignificant. Despite several studies highlighting the importance of non-equilibrium capillarity effects in unsaturated flow modeling, its significance in the mechanical response of the porous medium remains unclear. This study thus aims to address this gap by comparing the simulation results of the traditional static approach and an advanced approach that incorporates dynamic capillarity effects. The comparison is conducted under various flow boundary conditions to assess the magnitude of the differences between the two approaches. The results indicate that as the hydraulic boundary conditions' absolute values increase, the contrast between the mechanical response of the two simulation scenarios (dynamic and static) becomes more significant. For instance, the dynamic model can predict shear strengths up to 50% higher than the static model. This highlights the importance of considering non-equilibrium effects while modeling the mechanical behavior of an unsaturated porous medium. Finally, the parametric study of the effect of dynamic coefficient, air entry value, and saturated conductivity reveals the more pronounced effect of the dynamic coefficient on the mechanical response.

## 1 | INTRODUCTION

Multiphase flow in porous media is a physical process with a broad spectrum of applications in several disciplines, including geotechnical engineering, petroleum engineering, agriculture, fuel cells, and food science. In most of these

disciplines, a sound understanding of the coupled effects of flow and deformation is crucial to ensure an accurate design and a proper prediction of the system's behavior.

In common numerical simulations of water flow in unsaturated porous media, the degree of saturation is algebraically related to the pressure difference between the two fluid phases, namely, water and air, through the so-called retention

**Abbreviations:** BC, boundary condition; RC, retention curve.

This is an open access article under the terms of the [Creative Commons Attribution-NonCommercial-NoDerivs](https://creativecommons.org/licenses/by-nc-nd/4.0/) License, which permits use and distribution in any medium, provided the original work is properly cited, the use is non-commercial and no modifications or adaptations are made.

© 2024 The Authors. *Vadose Zone Journal* published by Wiley Periodicals LLC on behalf of Soil Science Society of America.

curves (RCs). These curves describe the dependency of the capillary pressure on the degree of saturation and are obtained experimentally. Analytical equations, such as those proposed in the pioneering works of van Genuchten (1980) and Brooks and Corey (1966), are used to incorporate these curves into the numerical simulations mathematically.

Two essential assumptions exist in the common procedure of unsaturated flow simulations described above. The first assumption is that in the macroscale, the capillary pressure is always assumed to be equal to the pressure difference between the two phases. The second assumption is inherent in the standard experimental procedure for acquiring RCs, which involves measuring equilibrium data points. In these experiments, a certain boundary condition is applied, and sufficient time is given for the sample to reach an equilibrium state before measurements take place. This implies that all data points are collected when the rate of change of hydraulic variables is almost zero, indicating that the air–water interfaces are static throughout the sample.

To elaborate on the first assumption, consider capillarity at the scale of an interface. The common definition of capillary pressure is introduced through Equation (1):

$$p_c = 2T_s K_m \quad (1)$$

In this equation,  $p_c$  denotes capillary pressure,  $T_s$  is the surface tension of water (liquid), and  $K_m$  is the mean curvature of the interface. Moreover, it is commonly written that:

$$p_c = p_a - p_w = p^{\text{diff}} \quad (2)$$

in which  $p_a$  and  $p_w$  represent air and water phase pressures, respectively, present on the two sides of the interface.

Hassanizadeh and Gray (1993) have argued that Equation (2) is true only under equilibrium conditions. To further discuss the distinction between capillary pressure and phase pressure difference (i.e.,  $p^{\text{diff}}$ ), consider a single capillary tube as depicted in Figure 1, where one fluid displaces another. Writing the balance of forces in the horizontal direction results in the following:

$$2T_s K_m = (p_a - p_w) - \mathbf{N} \cdot (\boldsymbol{\tau}^a - \boldsymbol{\tau}^w) \cdot \mathbf{N} \quad (3)$$

In the above equation,  $\boldsymbol{\tau}^a$  and  $\boldsymbol{\tau}^w$  are viscous stress tensors of the air and water phases, and  $\mathbf{N}$  is the unit vector normal to



FIGURE 1 A single interface between water and air in a capillary tube.

### Core Ideas

- Hydro-mechanical responses with and without considering dynamic capillarity are compared.
- Results are indicative of the significance of the effects of dynamic capillarity on hydro-mechanical behavior.
- Results are more sensitive to dynamic capillarity coefficient than saturated conductivity and air entry value.

the interface. Based on Equation (1), the left-hand side of this equation is equal to the capillary pressure, a definition that can be used under any conditions.

If the system is at equilibrium and the interface is not moving, the viscous stress tensors are zero, and Equation (3) reduces to Equation (2). However, if the system is in a dynamic state where the interface is moving, Equation (2) is no longer valid. According to Hassanizadeh and Gray (1993), capillary pressure is an intrinsic interface property and solely depends on its inherent properties. Therefore, the pressure difference alone cannot invariably define the value of the capillary pressure (Moeckel, 1975; Sheng & Zhou, 1992). Similar considerations can be extended to the macroscale.

Regarding the second assumption, numerous studies have indicated that the relationship between the  $p^{\text{diff}}$  and the degree of saturation is not uniquely defined, even when hysteresis effects are neglected. Hassanizadeh et al. (2002) have provided a review of such studies. An example of the studies that highlight this phenomenon has been conducted by Topp et al. (1967). In their research, they performed a series of experiments and demonstrated that the RCs vary with the rate of saturation change, making them distinct from the static curves obtained by measuring data points at suction equilibration. To monitor real-time changes in hydraulic variables, they utilized a tensiometer for suction measurement and a gamma-ray system for moisture measurement. Their findings have revealed that, compared to the static condition, during drainage, higher suction values are observed when the rate of desaturation is increased. Other researchers have subsequently confirmed the non-uniqueness of RCs for both drainage and imbibition paths, attributing it to variations in the rate of change of saturation (Bottero et al., 2011; Milatz et al., 2018; O'Carroll et al., 2005; Yan et al., 2024; Zhuang et al., 2017).

Numerous attempts have been made to comprehend the microscale origins of non-equilibrium effects. Diamantopoulos and Durner (2012), as well as Chen et al. (2022), have conducted a review of dynamic non-equilibrium effects. They have concluded that potential contributing mechanisms include the following microscale phenomena: relaxation of

air–water interfaces, limited air-phase permeability, dynamic contact angles, heterogeneity of soil properties at the measurement scale, time-dependent wettability changes, entrapment of water, pore water blockage, and air entry effects. Furthermore, they have stated that despite the availability of macro-scale observations, the current state of knowledge is insufficient to predictably quantify the importance of each microscale cause.

Although unraveling the microscale causes is still an ongoing research topic, various theories have been proposed to mathematically quantify the macroscale behavior. For instance, Hassanizadeh and Gray (1990, 1993) employed a thermodynamic approach and derived the following linearized equation:

$$P^{\text{diff}} = (P_a - P_w) = P_c - \tau \frac{\partial S_w}{\partial t} \quad (4)$$

where  $P^{\text{diff}}$  is the difference between the macroscale pressures of the air phase ( $P_a$ ) and the water phase ( $P_w$ ). It is worth mentioning that lowercase letters (used in Equations 1–3) are a common notation used in porous media studies to define microscale quantities, and capital letters (used hereafter) denote continuum scale quantities.  $S_w$  is the volume-averaged water phase degree of saturation,  $P_c$  stands for the capillary pressure that can be measured under equilibrium conditions and is a function of saturation,  $t$  is the time, and  $\tau$  denotes the dynamic capillarity coefficient. This coefficient is always positive, and its determination relies on experimental studies.

While the term RC commonly refers to the curves relating capillary pressure to the degree of saturation, for the sake of comparison, hereafter, in this manuscript, this term is generalized so that it stands for the relation between the phase pressure difference ( $P^{\text{diff}}$ ) and the degree of saturation. In this way, if the static assumptions are considered, RCs reflect the same definition as before and can be compared to those acquired from the dynamic formulation.

As evident from Equation (4), the pressure difference between the two phases is not solely determined by the degree of saturation but is also influenced by the rate of change of saturation; that is, as the absolute value of the rate of change of saturation increases, more significant deviation is expected between the real-time pressure difference measured at a certain saturation and the corresponding static capillary pressure. This can explain the shifts observed in RCs under non-equilibrium conditions, as reported in the literature, such as the study by Topp et al. (1967).

Considering the inconsistencies between traditional methods of two-phase flow in porous media and recent observations and theories, a question arises regarding the extent to which these differences affect the mechanical behavior of the porous medium. The contribution of the presence of multiple fluids in a porous medium to the mechanical behav-

ior is captured through the concept of effective stress (Fazli Ghiyasabadi et al., 2021; Huyghe et al., 2017; Khalili et al., 2004; Lu et al., 2014; Nikooee et al., 2012; Nikooee, Habibagahi, et al., 2013). Bishop (1959) has formulated the effective stress for a system of two immiscible fluids (such as air and water in an unsaturated soil) as presented in Equation (5). This equation emphasizes the crucial role played by the pressure difference between the air and water phases in controlling the changes in the effective stress.

$$\sigma' = (\sigma - P_a) + \chi (P_a - P_w) \quad (5)$$

In this equation,  $\sigma'$  is effective stress,  $\sigma$  is total stress, and  $\chi$  represents the effective stress parameter.

Based on Equation (5), it can be presumed that any variation in the pressure difference may cause a significant change in the effective stress, and, consequently, impact the mechanical behavior of the medium. As mentioned in the literature, dynamic conditions can lead to variations in both the degree of saturation and the pressure difference, further affecting the effective stress values.

Although the changes in the stress field resulting from dynamic effects may seem trivial, the overall importance and the magnitude of such changes remain unclear, and few attempts have been made to address this issue. By combining Equations (4) and (5), Nikooee, Hassanizadeh et al. (2013) proposed the following equation for the effective stress under non-equilibrium conditions:

$$\sigma' = \sigma - P_a + \sigma_s = \sigma - P_a + \chi \left( \psi_m - \tau \frac{\partial S_w}{\partial t} \right) \quad (6)$$

where  $\psi_m$  denotes matric suction and  $\sigma_s$  is suction stress.

Later, Milatz et al. (2018) utilized the abovementioned equation to estimate the changes in suction stress in their transient flow experiment on a sandy soil called ISS0-sand. They conducted a series of imbibition and drainage tests on cylindrical sand samples under both quasi-static and transient conditions, successfully capturing the non-equilibrium effects in unsaturated flow (Figure 2). By fitting the experimental data, they have discovered a linear relationship between the parameters  $\tau$  and  $S_w$ .

Yan et al. (2022) have recently conducted a comprehensive review of transient two-phase flow in porous media and its application in geotechnical engineering. They have concluded that the lack of experimental data regarding coupled transient flow and deformation might stem from the challenges associated with conducting such tests. Evaluating the effect of transient flow on the mechanical behavior of soils necessitates a specialized apparatus capable of imposing transient flow boundary conditions while simultaneously applying mechanical loading. Furthermore, real-time measurements of both the system's hydraulic and deformation responses must be carried out during the tests.

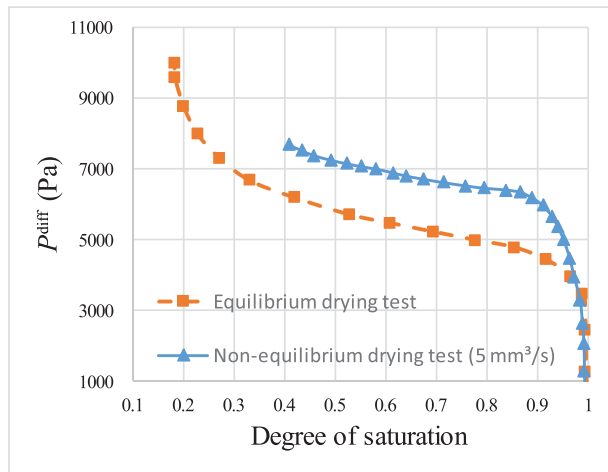


**FIGURE 2** Static and dynamic retention curves for ISS0-sand (Milatz et al., 2018).

Since developing or having access to the necessary specialized apparatus for experimental testing is challenging, numerical simulations can be employed as a viable alternative to investigate the potential effects of dynamic capillarity on the mechanical behavior of samples. Numerical simulations provide a virtual laboratory for testing and allow for exploring various aspects of dynamic capillarity.

Furthermore, traditional techniques are inefficient in providing a comprehensive understanding of the spatial distribution of water within a sample. While advanced techniques like magnetic resonance imaging or electro resistivity tomography can offer more accurate measurements of local water distributions (Cosentini et al., 2012; Guo et al., 2023), they are not suitable for capturing fast changes inherent to transient phenomena. Therefore, numerical simulations remain the primary method for studying local moisture distribution across a sample.

To address the limitations of the existing literature, in this study, the governing equations that describe the unsaturated flow along with the soil mechanical responses were employed to assess the potential effects of non-equilibrium conditions on the mechanical behavior of sandy soils. First, the flow model was verified, and subsequently, it was coupled with a mechanical framework to examine the shear strength of unsaturated samples under the triaxial loading, considering the dynamic capillarity effects. To the best of the authors' knowledge, no comparable study has been reported in the literature.

## 2 | METHODOLOGY AND FORMULATION

To investigate the potential effects of dynamic capillarity on the mechanical behavior of sandy soils, a numerical

simulation was conducted to model two phenomena simultaneously: transient unsaturated flow in the porous medium and the mechanical response of the medium to an external load. The governing equations for both phenomena were solved over a domain using the partial differential equations module of COMSOL Multiphysics software. These two phenomena were simulated in a one-way-coupled manner, which means that while the influence of flow on mechanical response was taken into account, the changes in hydraulic state and parameters associated with the sample deformation were considered negligible. In support of this assumption, it is crucial to emphasize that the peak shear strength of the samples was investigated in this study. Since reaching this stress state requires small strain values, it was assumed that the impact of medium deformation on the porous structure and, consequently, the hydraulic state is likely minimal.

### 2.1 | Flow model

The flow was simulated using two scenarios. In the first scenario, referred to as the static flow formulation, the commonly used formulation for two-phase flow in porous media was employed to calculate the pressure and saturation distribution during the sample drainage from an initially fully saturated state. In this scenario, the phase pressures ( $P_a$  and  $P_w$ ) were determined numerically, and their difference was set equal to the capillary pressure. Moreover, capillary pressure was assumed to be uniquely related to the effective saturation, as prescribed by the van Genuchten equation in the studied drying process.

For the second scenario, in the general governing equations of flow, the difference in pressure of phases should satisfy the dynamic equation, as presented by Equation (4). In this scenario, the variable  $P_c$  was considered a function of the degree of saturation calculated by van Genuchten's formulation and did not necessarily take the value of the difference in fluid phase pressures. This scenario was called dynamic flow formulation. The system of equations for each scenario is presented in Table 1. For the sake of comparison, all the other variables and conditions were kept the same for both scenarios.

It is noteworthy that although Richards' equation is commonly employed for numerical simulation of unsaturated flow in soils, this equation was not used here. Due to the known numerical issues of Richards' equation and to avoid non-physical saturation profiles, the mass balance equations were solved for air and water phases in both scenarios. However, the variation in air pressure throughout the sample remained insignificant.

The soil used in this study was a fine-grained sand called ISS0-sand, and its hydraulic properties are presented in

TABLE 1 System of equations for dynamic and static scenarios.

	Static formulation	Dynamic formulation
Dependent variables	$P_a$ and $P_w$	$P_a$ , $P_w$ , and $S_w$
Mass balance equation	$\varphi \rho_i \frac{\partial S_w}{\partial t} + \nabla \cdot (\rho_i q_i) = 0$ & $i = a, w$	$\varphi \rho_i \frac{\partial S_w}{\partial t} + \nabla \cdot (\rho_i q_i) = 0$ & $i = a, w$
Discharge rate	$q_i = -K^i \nabla \left( \frac{P_i}{\rho_i g} + z \right)$	$q_i = -K^i \nabla \left( \frac{P_i}{\rho_i g} + z \right)$
Permeability	$K^i = K_r^i \times K^{\text{Sat}, i}$ $K_r^w = S_e^{\frac{2+3\lambda}{\lambda}}$ , $K_r^a = (1 - S_e)^2 (1 - S_e^{\frac{2+\lambda}{\lambda}})$	$K^i = K_r^i \times K^{\text{Sat}, i}$ $K_r^w = S_e^{\frac{2+3\lambda}{\lambda}}$ , $K_r^a = (1 - S_e)^2 (1 - S_e^{\frac{2+\lambda}{\lambda}})$
Capillarity equation	$(P_a - P_w) = P_c$	$(P_a - P_w) = P_c - \tau \frac{\partial S_w}{\partial t}$
Retention model	$P_c = \frac{1}{\alpha} \left( \sqrt[n]{S_e} - 1 \right)^{1/n}$ , $m = 1 - \frac{1}{n}$	$P_c = \frac{1}{\alpha} \left( \sqrt[n]{S_e} - 1 \right)^{1/n}$ , $m = 1 - \frac{1}{n}$
Effective saturation	$S_e = \frac{S_w - S_w^{\text{res}}}{1 - S_w^{\text{res}}}$	$S_e = \frac{S_w - S_w^{\text{res}}}{1 - S_w^{\text{res}}}$

TABLE 2 Hydraulic properties of the soil (Milatz et al., 2018).

Parameters	Value	Explanation
$\alpha$ (1/kPa)	0.174	van Genuchten parameter
$n$	9	van Genuchten parameter
$m$	0.89	van Genuchten parameter
$K^{\text{sat}}$ (m/s)	1.2e-4	Saturated hydraulic conductivity
$\varphi$	0.444	Porosity
$S_w^{\text{res}}$	0	Residual saturation
$\lambda$	3.96	Brooks-Corey parameter
$P_d$ (kPa)	4.723	Brooks-Corey parameter
$\tau$ (Pa · s)	5.28e6 – 0.379e6 $\times S_w$	Dynamic coefficient

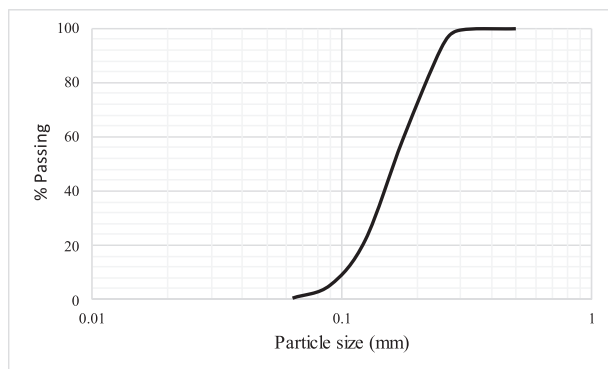


FIGURE 3 Particle size distribution of the ISS0-sand as reported by Milatz et al. (2018).

Table 2, as reported by Milatz et al. (2018). The particle size distribution of this sand is also shown in Figure 3.

In our hydro-mechanical simulations, the sample was assumed to be cylindrical in shape with a height of 200 mm and a diameter of 100 mm. The axisymmetric assumption was employed due to the symmetrical geometry and the bound-

ary conditions. Boundary conditions (BCs) for the air phase were no-flow on the walls and the bottom of the cylinder and an atmospheric pressure at the top boundary. For the water phase, to the top boundary and the walls, no-flow condition was assigned, and at the bottom boundary, two sets of BCs were considered, a flowrate boundary condition and a pressure boundary condition, applied in distinct simulations (see Figure 4). Different values considered for the bottom BCs are presented in Table 3.

All flow models started from the same initial condition, irrespective of the formulation scenario or the boundary condition. This initial condition was acquired from the results of a steady-state analysis prior to the main simulations, in which the water table was assumed to be at the bottom of the sample. As a result, considering the sand's air entry value and the column's height, the entire sample would be fully saturated while the capillary pressure was non-zero (i.e., capillary fringe zone). This steady-state preprocess ensured consistency in the subsequent simulations' initial conditions.

A time-dependent study was conducted for the transient flow model, in which the simulation time was set as follows: for the models with pressure boundary conditions, the simulation time was sufficiently long for the model to pass through the transient phase and reach a final equilibrium state, and for the models with flowrate boundary condition, the model was kept running as long as the saturation in all model elements was higher than a certain value. This condition was set to avoid convergence issues. The results from the flow model representing the values and distribution of all hydraulic variables were then used in the subsequent mechanical model.

The simulation was carried out using the partial differential equation (PDE) module of COMSOL Multiphysics software. The spatial discretization for both flow and mechanical models was done using a quadratic mesh with a maximum dimension of 0.5 cm and a cubic Lagrange shape function (see Figure 4). This choice of element shape and order proved

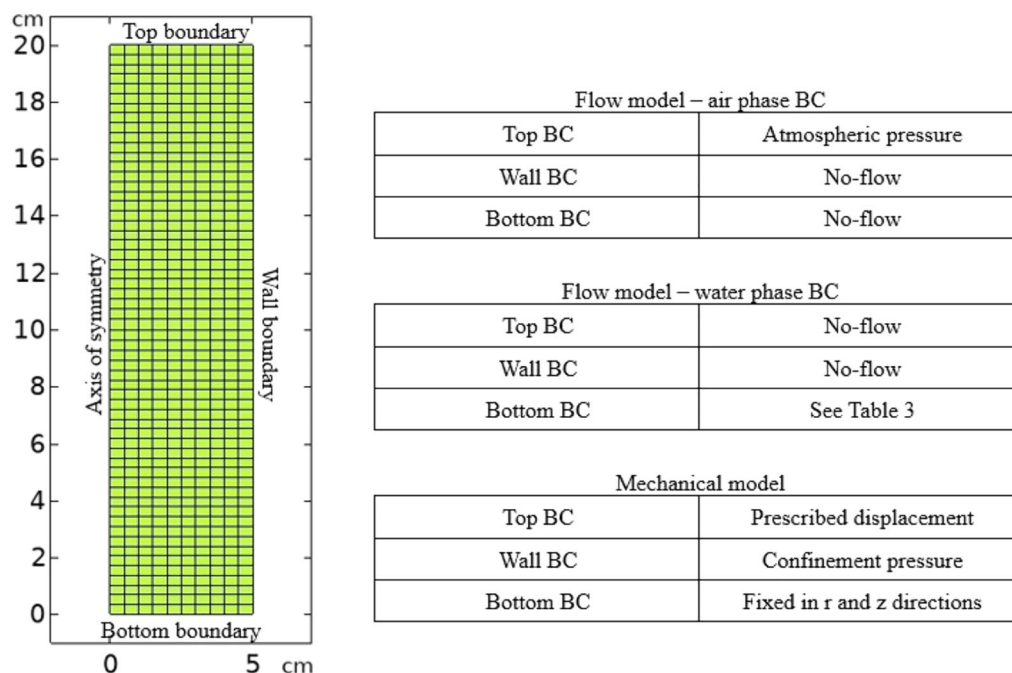


FIGURE 4 Spatial discretization and boundary conditions. BC, boundary condition.

TABLE 3 Value and types of boundary conditions applied to the bottom boundary.

BC numbering	BC type	Value
p-I	Water pressure	−2.5 kPa
p-II	Water pressure	−5.0 kPa
p-III	Water pressure	−7.5 kPa
f-I	Outflowrate	25 mm <sup>3</sup> /s
f-II	Outflowrate	50 mm <sup>3</sup> /s
f-III	Outflowrate	150 mm <sup>3</sup> /s
f-IV	Outflowrate	250 mm <sup>3</sup> /s

Abbreviation: BC, boundary condition.

adequate for reaching convergence, considering the governing equations' high level of non-linearity. The backward differentiation formula (BDF) solver was used for the time stepping due to its proven stability. The BDF solver adjusted the time steps automatically to achieve convergence based on the mesh size, relative tolerance factor, and BDF order.

## 2.2 | Verification of dynamic flow model

To ensure the proper functioning of the dynamic flow model, the output of this model was initially verified using experimental results. For this purpose, the Milatz et al. (2018) experiment was used as a benchmark. The soil hydraulic properties employed in the simulation are provided in Table 2. In this experiment, an out-flowrate boundary condition of

5 mm<sup>3</sup>/s was imposed at the bottom of a cylindrical specimen with a diameter of 40 mm and a height of 20 mm.

For the purpose of comparison, both static and dynamic formulations were utilized to simulate the benchmark experiment with the same boundary and initial conditions. The results of the verification test are presented in Section 3.

## 2.3 | Mechanical model

The ultimate goal of this study was to gain insight into the magnitude and significance of dynamic capillarity effects on the sandy soils' mechanical behavior. Therefore, a comparison index for the mechanical properties was needed to be chosen. The maximum deviatoric stress (i.e., the difference between the axial and radial stresses imposed on the triaxial model) that could be withstood at different hydraulic states reached in the drainage process was selected as the index. The values of the maximum deviatoric stress at different time instances for the two simulation scenarios, namely, dynamic and static formulations, were calculated and reported. In doing so, after executing the flow models, the values of all hydraulic parameters were extracted from the flow model and then imported into the mechanical model for several selected points in time. Equation (5) was used, assuming  $\chi = S_w$  to relate the hydraulic and mechanical states (Bishop, 1959; Khalili et al., 2022). At this stage, each mechanical model represented a consolidated constant water content test with the hydraulic state corresponding to the selected time instance and formulation. Solving the mechanical model would result

TABLE 4 Mechanical properties of the soil.

Parameters	Value	Explanation
C (kPa)	0.1	Cohesion
$\phi$ (°)	34	Friction angle
E (MPa)	20	Elastic modulus
$\nu$	0.33	Poisson's ratio
$\gamma_d$ (kN/m <sup>3</sup> )	18	Dry unit weight

in a curve of deviatoric stress ( $q$ ) versus axial strain ( $\epsilon$ ) at that time instance.

The loading phase was simulated using the solid mechanics module of COMSOL Multiphysics. The bottom boundary was fixed in both directions ( $r$  and  $z$ ). First, the sample was exposed to a confining pressure, and then it was loaded by applying a prescribed displacement at the top boundary while the surrounding confinement was maintained. Simultaneously, the deviatoric stress mobilized at the top boundary was measured and recorded. Steady-state mechanical analysis was employed to incrementally impose a stepwise displacement at the top boundary, obtaining a point on the deviatoric stress versus axial strain curve at each step. The maximum value from this curve represented the mechanical response of the sample at the given hydraulic state. These maximum values were then plotted against time for both static and dynamic formulations, allowing for comparison and interpretation.

The confining pressure was set to 5 kPa for all tests. Additionally, a couple of simulations were performed to assess the potential effects of confinement on the significance of dynamic capillarity effects, in which a higher value of confining pressure, namely, 10 kPa, was taken. The mechanical response was determined based on a Mohr–Coulomb failure criterion. Further details regarding the governing equations have been provided by Davis and Selvadurai (2005) and Pryor (2009). The selected Mohr–Coulomb and elastic parameters are presented in Table 4.

## 2.4 | Parametric study of the influence of hydraulic parameters

Many studies have been carried out to investigate the impact of different hydraulic parameters on the extent of dynamic capillarity effects for two-phase flow phenomena. However, few attempts have been made to take another step forward and study the effect of each hydraulic parameter on the soil's mechanical response under non-equilibrium flow conditions. With that in mind and given the relatively smaller number of dynamic non-equilibrium experiments compared to traditional equilibrium ones, a parametric study would provide us with a better understanding of the impact of each parameter in this context. For this purpose, three parameters were examined in this section: dynamic coefficient ( $\tau$ ), saturated

TABLE 5 The range of soil variables as reported by Griffiths and Lu (2005).

Soil type	$\alpha$ (1/kPa)	$K^{sat}$ (m/s)
Sand	0.1–0.5	$10^{-2}$ to $10^{-5}$

hydraulic conductivity ( $K^{sat}$ ), and van Genuchten  $\alpha$ -parameter (as a surrogate for air entry pressure). The selected range for the latter two was considered to match the reported range in the literature (Table 5). Additionally, the range of dynamic coefficient was assumed based on the reported values of Hassanizadeh et al. (2002) and Li et al. (2022), where the reported values for sand have been as low as  $10^4$  Pa·s (Goel & O'Carroll, 2011; Mirzaei & Das, 2007) and as high as  $10^9$  Pa·s (Sakaki et al., 2010).

Table 6 shows the different values of the hydraulic subject variables. Level 2 values were considered the same as the soil used in previous sections (ISS0-sand), and Levels 1 and 3 were chosen to represent an upper and a lower value for the subject parameters. In this study, only one subject variable value was changed for each examination, while all the other variables were kept constant and equal to the original values of the soil (Level 2). These nine simulations' outcomes are presented and compared in the results section.

## 3 | RESULTS AND DISCUSSION

In this section, first, the results of the verification process are presented. Then, the outputs of the flow model are discussed. It is followed by the findings of mechanical simulation, where the effect of different scenarios, dynamic versus static flow simulations (as well as hydraulic boundary conditions) on the mechanical response of the soil is examined. Finally, the results of the parametric study are reported and further discussed.

### 3.1 | Verification results

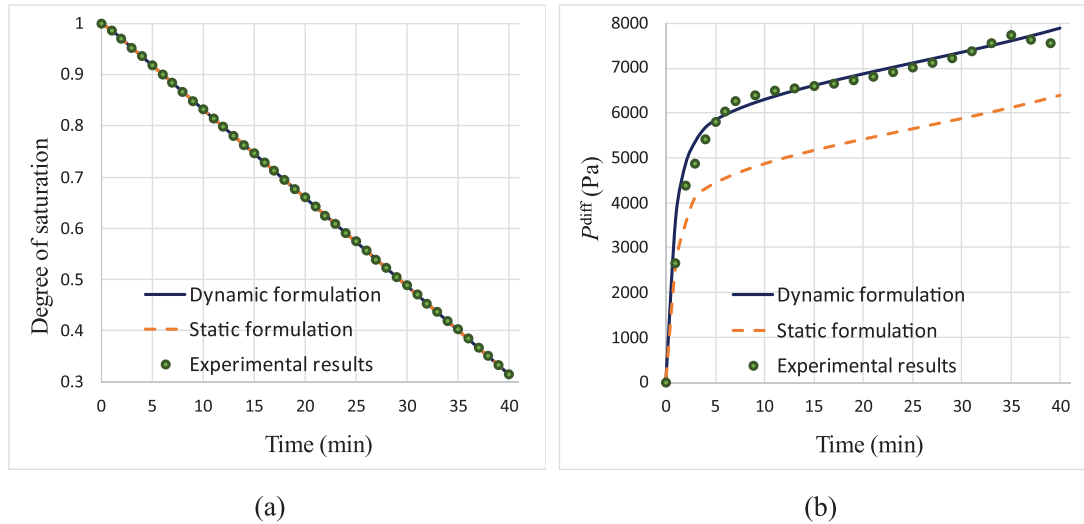
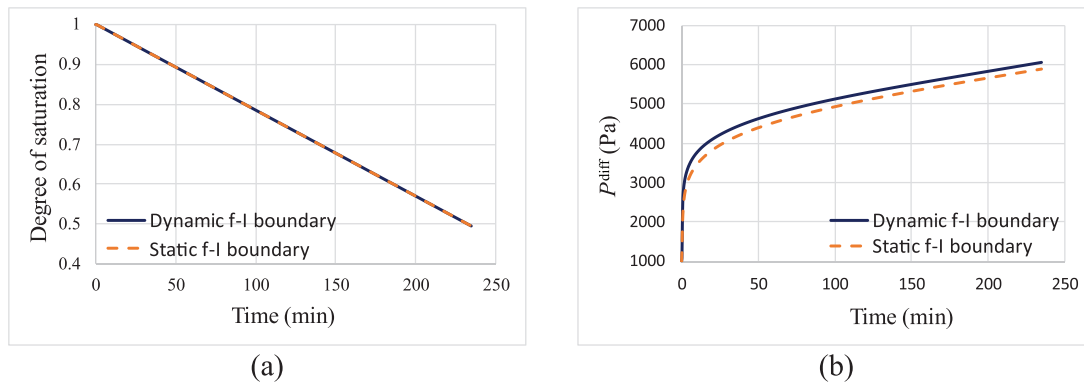
The experimental data points of the degree of saturation and pressure difference values reported by Milatz et al. (2018) are presented in Figure 5, along with the simulation values (for the ISS0-sand sample).

As can be seen in Figure 5a, the changes in the degree of saturation were the same for both static and dynamic simulations, matching the experiments very well. This behavior can be expected as the boundary condition was a specified flowrate, we had a one-dimensional flow, and both formulations and their numerical implementation satisfied the conservation of mass. However, the static formulation failed to follow the pressure difference of the two phases ( $P^{diff}$ ), whereas the dynamic formulation showed a very good agreement with the

**TABLE 6** Values of subject variables for the parametric study.

Subject variable	Level 1	Level 2	Level 3
$\tau^a$ (Pa·s)	$5.28e5 - 0.379e5 \times S_w$	$5.28e6 - 0.379e6 \times S_w$	$5.28e7 - 0.379e7 \times S_w$
$K^{sat}$ (m/s)	$1.2e-3$	$1.2e-4$	$1.2e-5$
$P_d$ (kPa)	3.723	4.723	5.723

<sup>a</sup> $\tau$  is assumed to take the same functionality of saturation as the one reported by Milatz et al. (2018). However, its abscissa was varied to change the values in a range comparable to the literature.

**FIGURE 5** Experimental data and simulation results of the benchmark experiment.**FIGURE 6** Results of flow simulation of boundary condition (BC) f-I ( $25 \text{ mm}^3/\text{s}$ ) for static and dynamic formulation.

experimental data. As mentioned previously, the only difference between these two scenarios was the inclusion of the dynamic capillarity equation in the system of equations.

### 3.2 | Results of flow model

The flow model results for the two formulation scenarios were expressed as curves depicting phase pressure difference ( $P^{diff}$ ) and saturation versus time. In addition, by plotting the phase pressure difference against the degree of saturation, the RCs of related tests were also presented.

Figures 6–9 show the results of both static and dynamic formulations for four values of outflowrate BCs from 25 to  $250 \text{ mm}^3/\text{s}$ . In these tests, the plots of saturation versus time for both formulations coincided following the same reasoning mentioned for the verification results (i.e., the imposed BC was of the flowrate type, and both formulations were mass conservative). In contrast,  $P^{diff}$  values versus time were different, with the difference increasing with larger flowrates.

Figures 10–12 show the pressure BC results for static and dynamic formulations. In contrast to the flow boundary type, the main difference was mainly in the curves of saturation versus time. As evident from the graphs, the change in

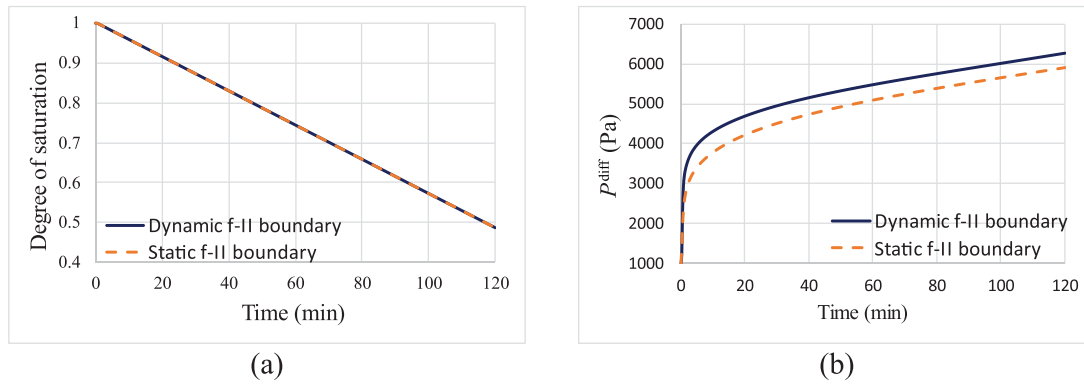


FIGURE 7 Results of flow simulation of boundary condition (BC) f-II ( $50 \text{ mm}^3/\text{s}$ ) for static and dynamic formulation.

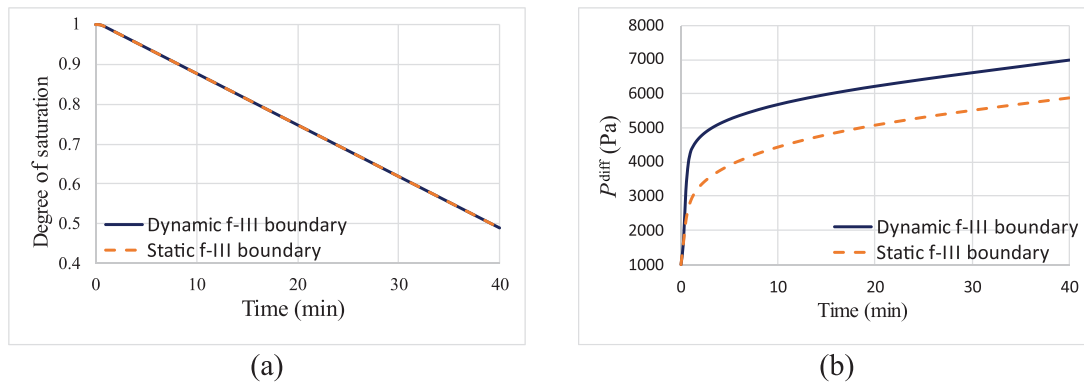


FIGURE 8 Results of flow simulation of boundary condition (BC) f-III ( $150 \text{ mm}^3/\text{s}$ ) for static and dynamic formulation.

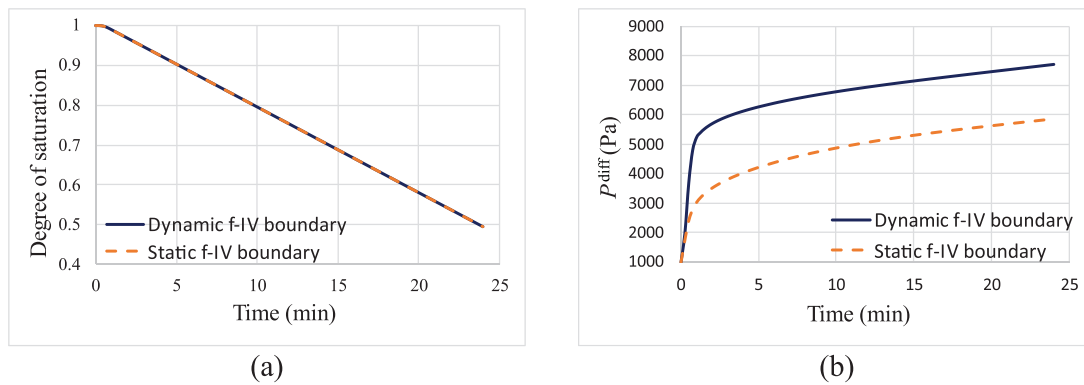


FIGURE 9 Results of flow simulation of boundary condition (BC) f-IV ( $250 \text{ mm}^3/\text{s}$ ) for static and dynamic formulation.

saturation happened more gradually in the dynamic formulation than in the static formulation. In other words, in the dynamic scenario, the dynamic coefficient ( $\tau$ ) acted like a damping factor, which was in agreement with the findings in the previous studies (Manthey et al., 2005; Mirzaei & Das, 2013; Sakaki et al., 2010).

Having examined the variation in the  $P^{\text{diff}}$  with time, a different trend was observed at the higher imposed pressure BCs, as depicted in Figure 12b. For p-III BC, a peak in the  $P^{\text{diff}}$ -time curve was observed at the beginning of the sim-

ulation. It then gradually leveled off, eventually approaching the phase pressure difference obtained from the static formulation. A possible cause might be the abrupt change in the saturation at the beginning of the test. As mentioned earlier, all tests started from the condition of full saturation. By imposing the pressure boundary condition, the desaturation rate was observed to increase to a maximum value, and when the model reached equilibrium, it was eventually reduced to zero (see Figure 13). On the other hand, since the degree of saturation was monotonically decreasing,  $P_c$  would always be

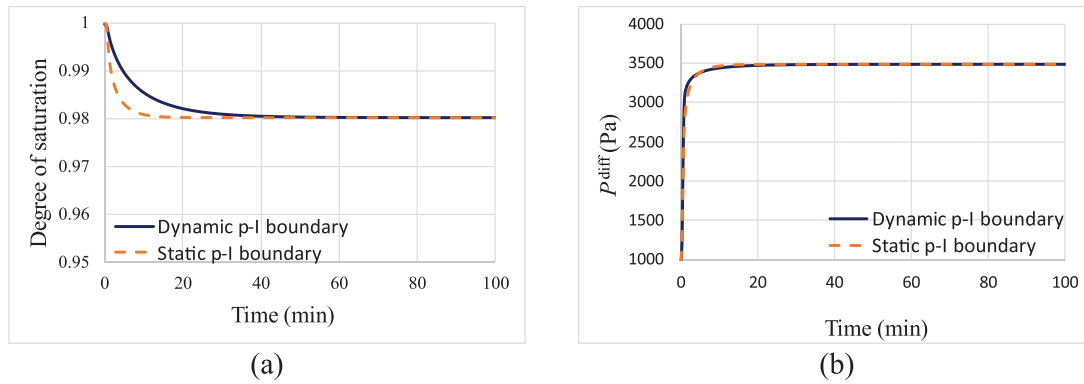


FIGURE 10 Results of flow simulation of boundary condition (BC) p-I ( $-2.5$  kPa) for static and dynamic formulation.

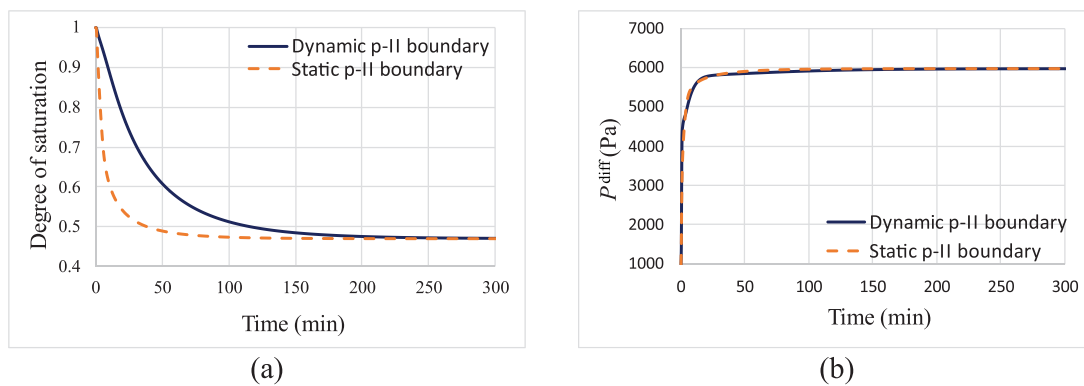


FIGURE 11 Results of flow simulation of boundary condition (BC) p-II ( $-5.0$  kPa) for static and dynamic formulation.

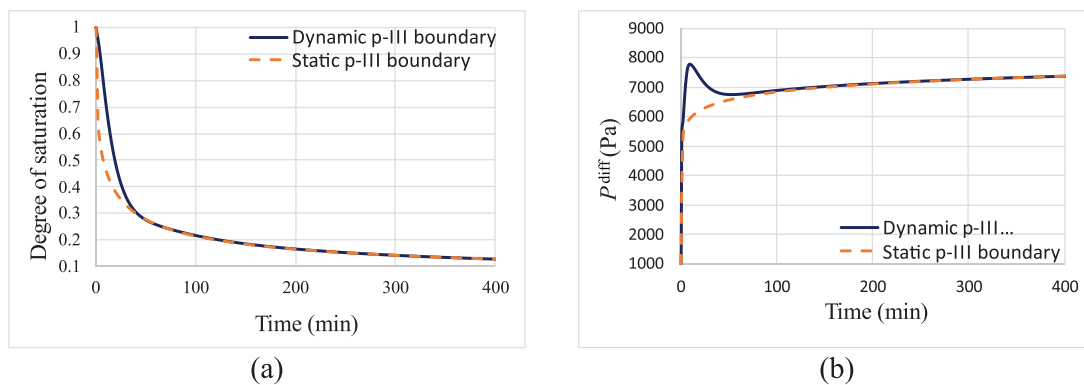
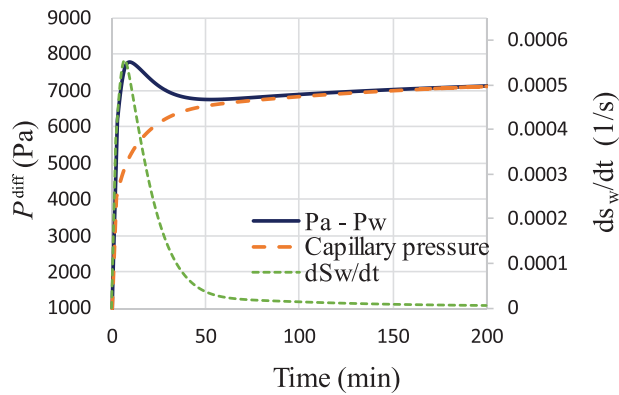


FIGURE 12 Results of flow simulation of boundary condition (BC) p-III ( $-7.5$  kPa) for static and dynamic formulation.

increasing. In this particular test, the water pressure change applied as the boundary condition was as high as  $-7.5$  kPa, or about 80% of the static soil water retention curve's (SWRC) residual suction imposed in a single step. This substantial change in the suction resulted in a significant change in saturation, that is, a large value of  $|\frac{\partial S_w}{\partial r}|$  at the early stages of the test. Based on Equation (4), this number was large enough to create a peak in the value of the pressure difference between phases. The non-monotonicity of phase pressure difference as a result of extreme boundary conditions has also

been observed in experimental studies such as those reported by Camps-Roach et al. (2010) and Bottero et al. (2011).

For each test, the dynamic RCs were obtained by plotting the pressure difference against the degree of saturation. From Figures 14 (for flowrate BC) and 15 (for pressure BC), it can be inferred that the dynamic formulation exhibited noticeable changes in saturation–pressure difference, whereas the outcome of the static formulation remained constant regardless of the boundary condition value. Curves very similar to those shown in Figure 15 have been reported by Bottero et al. (2011)



**FIGURE 13** Changes in the rate of change of saturation, capillary pressure, and pressure difference in dynamic formulation for boundary condition (BC) p-III.

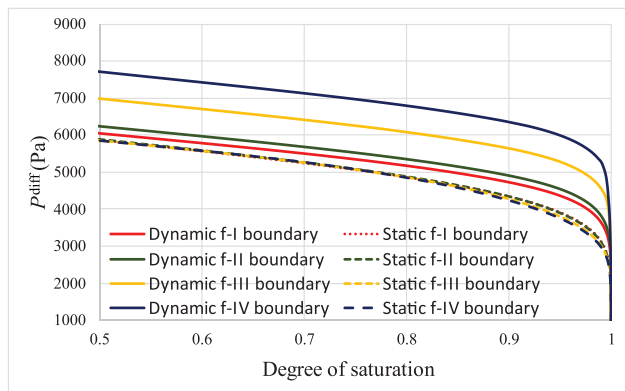


**FIGURE 14** Retention curves (RCs) obtained from dynamic and static formulation for the flowrate boundary conditions (BCs).

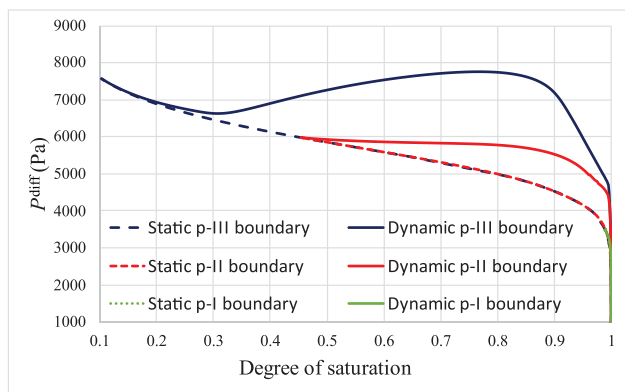


**FIGURE 15** Retention curves (RCs) obtained from dynamic and static formulation for the pressure boundary conditions (BCs).

from the results of the column experiments, which also had pressure boundary conditions.

Aside from significant differences in the values of saturation and phase pressures, the simulation results also showed noticeable differences in local water saturation distribution. Most interestingly, in the flowrate BC models, while the aver-

age saturation was identical for both formulation scenarios, the distribution of water inside samples was not the same for the two formulations. For instance, Figure 16 shows the water saturation distribution at  $t = 10$  min for f-IV BC for static and dynamic scenarios. Although both models had an average degree of saturation equal to 0.8, in the static scenario, local water saturation varied from 0.5 up to 0.97, whereas the dynamic scenario resulted in a narrower range spanning from 0.64 to 0.9. Similar trends can also be seen in pressure BC models.

### 3.3 | Results of triaxial simulation (mechanical model)

Since the hydraulic state strongly affects the soil mechanical response through the effective stress equation, any change in the distribution of phase pressures and/or degree of saturation is expected to alter the mechanical behavior. By utilizing the procedure mentioned in the methodology section for mechanical loading, the shear response of the samples was investigated at each time instance, as described below.

First, shear stress–strain responses (expressed in terms of  $q$ - $\epsilon$  curves) were obtained for various points in time. Figure 17 shows a typical result for BC type f-III. As the figure reveals, the general behavior of both scenarios followed the same pattern. However, in the dynamic formulation, the maximum deviatoric stress, a measure of the shear strength, was about 20% higher than the corresponding value in the static case. Furthermore, our study showed that the volumetric strain at peak shear strength was low as expected (e.g., it reached the value of 0.04% at  $t = 2$  min for f-III BC with dynamic scenario). The limited change in volume further justified our one-way coupling assumption.

Repeating the same loading test for multiple points in time and recording the maximum deviatoric stress, a  $q^{\max-t}$  curve was acquired for each BC of the two scenarios. Those results are presented in Figure 18. In the same figures, the difference between the maximum deviatoric stress determined from dynamic and static formulations ( $\Delta q^{\max} = q_{\text{dyn}}^{\max} - q_{\text{stat}}^{\max}$ ), normalized by the value of  $q_{\text{stat}}^{\max}$  have been shown. This “normalized difference” indicates the mechanical significance of the dynamic formulation, which is seldom used in geotechnical studies.

In the BCs with smaller pressure change or flowrate values, such as f-I or p-I, the mechanical response of both formulations (i.e., dynamic and static) was the same, with a normalized difference of <5%. These simulations’ boundary values were close to typical values in traditional SWRC tests (quasi-static approaches such as a standard pressure plate test). Therefore, the differences were insignificant. As the BC took higher values in each test, the deviation between the mechanical response of static and dynamic formulation

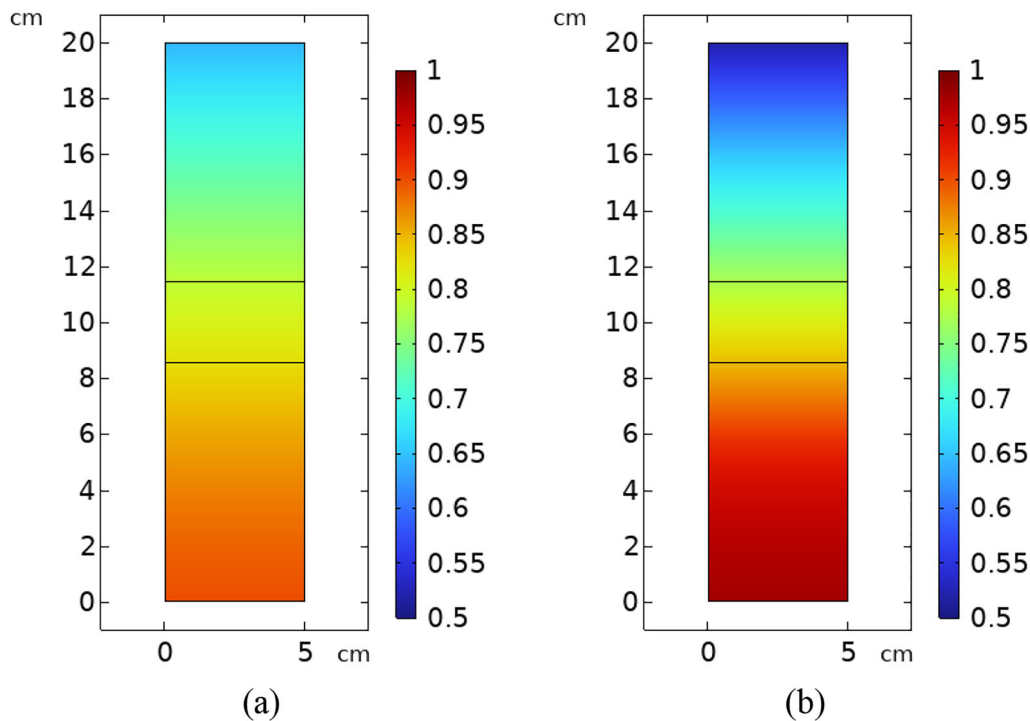


**FIGURE 16** Distribution of water saturation at  $t = 10$  min from simulations with flowrate boundary condition (BC): (a) dynamic scenario; (b) static scenario.

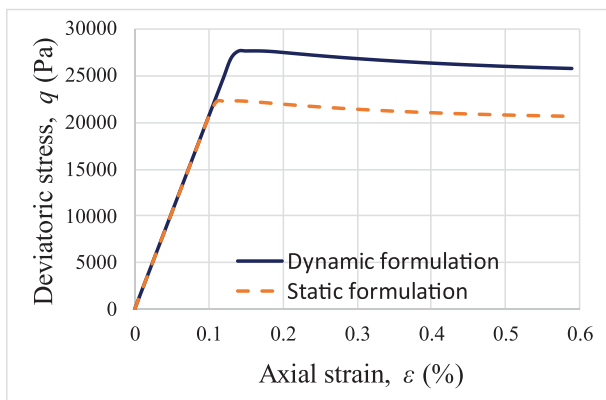


**FIGURE 17**  $q$ - $\epsilon$  curve for static and dynamic scenarios at  $t = 2$  min for f-III boundary condition (BC).

became more pronounced up to a certain point in time, surpassing which they started converging.

This convergence in the final stages of mechanical simulation seemed trivial for the pressure BCs, as for this boundary type, the flow models had also converged toward equilibrium in the late stages (see Figures 10–12). Additionally, for both flowrate and pressure BCs following Equation (6), the contribution of pressure difference to the effective stress consisted of pressure difference multiplied by the degree of saturation (taken as the effective stress parameter therein). Therefore, although the pressure difference value for each formulation increased, the overall contribution of suction stress would

diminish; as a result, the maximum shear stress resulting from both formulations converges eventually.

Moreover, it should be highlighted that the normalized difference between dynamic and static maximum deviatoric stress values took considerable values, as much as almost 40% and 50%, obtained for f-IV and p-III tests, respectively (as evident from Figure 18d,g).

Such results may have substantial implications in engineering practice, where the dynamic capillarity can influence the mechanical response. This can be the case in the stability analysis of the upstream slope of earth dams under rapid drawdown or rapid fill-up conditions, rainfall-induced landslides, etc. The extension of the simulations performed in this study to large-scale simulations of earth dams and slopes is encouraged as the subject of future studies.

### 3.4 | Effect of confinement on the significance of dynamic capillarity effect on the soil mechanical behavior

In practice, the confining pressure implies the field stress that a soil sample is experiencing at a particular depth. In order to inspect how this parameter can influence the difference between mechanical models coupled with static and dynamic capillarity formulations, the value of confining pressure was increased from 5 to 10 kPa for BC types f-III and p-II. The

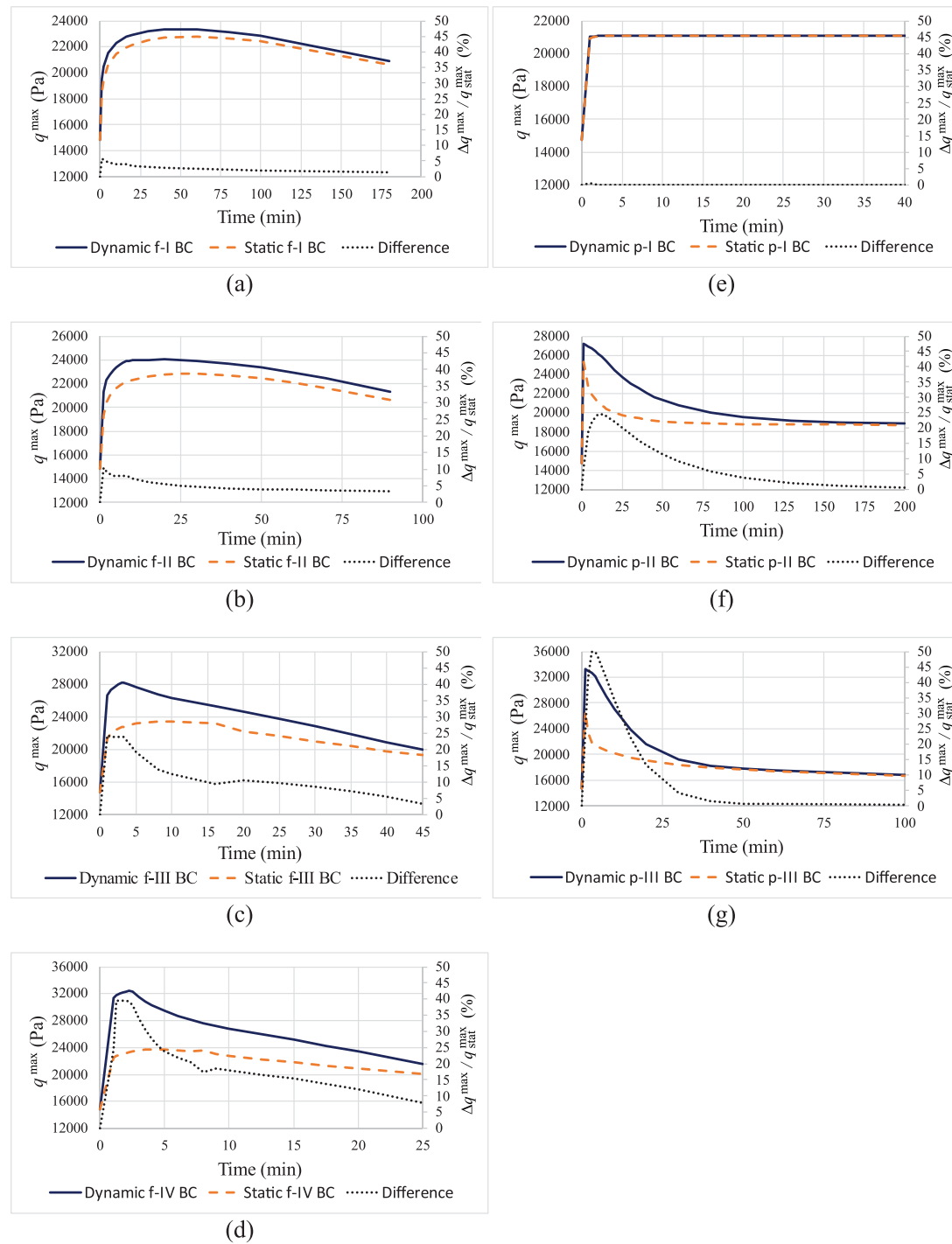


**FIGURE 18** Mechanical results of both static and dynamic formulations with 5 kPa confining pressure for the seven boundary conditions: f-I (a), f-II (b), f-III (c), f-IV (d), p-I (e), p-II (f), and p-III (g). BC, boundary condition.

mechanical responses were re-evaluated, and the results are presented in Figure 19.

Our results showed that the normalized difference between dynamic and static shear stress decreased for larger confining pressure. For instance, at  $t = 3$  min, the maximum shear stress acquired from BC type f-III with confinement value of 5 kPa were 28.2 and 22.8 kPa for dynamic and

static cases, respectively; their normalized difference was 24%. By increasing confinement to 10 kPa at  $t = 3$  min, the abovementioned values were increased to 40.8 and 35.3 kPa, respectively; their difference was only 15%. This implies that the significance of the dynamic effect on mechanical response would reduce with the increase of confining pressure.

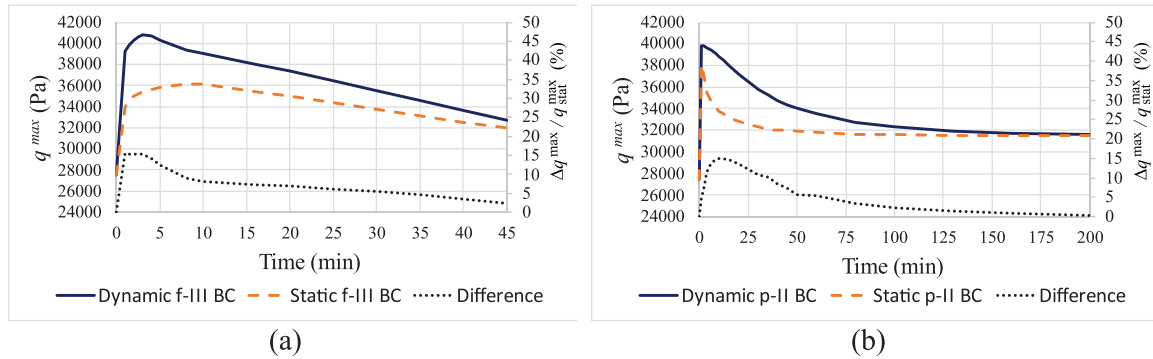


**FIGURE 19** Mechanical results of both static and dynamic formulations with 10 kPa confining pressure for f-III boundary condition (BC) (a) and p-II BC (b).

The same trend can be obtained by comparing Figures 18f and 19b (mechanical results of p-II BC for 5 and 10 kPa of confinement, respectively). This reduction implies that consideration of dynamic capillarity is of more importance in near-surface geological hazards such as shallow failure of embankment slopes.

### 3.5 | Results of the parametric study

The results of a sensitivity study for different hydraulic parameters are presented hereafter. The values of dynamic capillarity coefficient, saturated hydraulic conductivity, and air entry pressure (actually, van Genuchten  $\alpha$ -parameter) were individually varied, as shown in Table 6. For the sake of comparison and also since the main objective was to unravel the importance of non-equilibrium effects, the results are presented in terms of curves of normalized difference ( $\frac{\Delta q_{max}}{q_{stat}}$ ) versus time.

#### 3.5.1 | Effect of dynamic coefficient

Three levels were considered for the dynamic coefficient based on Table 6. Levels 1 and 3 were one order of magnitude smaller and larger than Level 2 (original value of ISS0-sand), respectively. The results, shown in Figure 20, indicated that  $\tau$  has directly influenced the normalized differences in maximum shear stress. Adding one order of magnitude to the original value of the dynamic coefficient resulted in increasing the normalized difference in maximum shear stress from about 25% to 35%, while reducing it dropped the normalized difference from 25% to just below 10%. Moreover, larger values of  $\tau$  resulted in much longer mechanical equilibrium time. As evident from Figure 20, for the lowest range of  $\tau$  values (Level 1), the normalized differences reached equilibrium in about 75 min. In contrast, the simulation with the highest value of  $\tau$  (Level 3) was still far from equilibrium after 250 min of simulation.

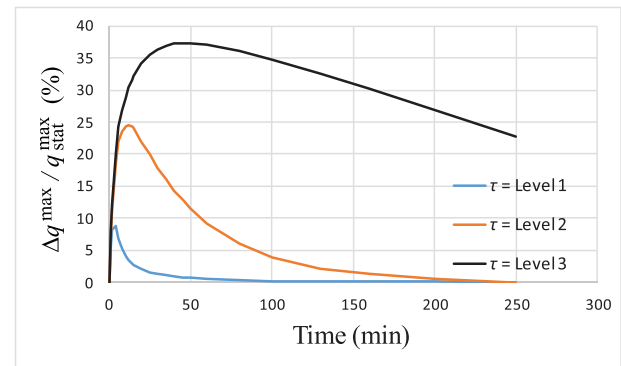


**FIGURE 20** The results of the parametric study: the effect of the dynamic coefficient on the normalized difference in the maximum shear stress ( $K^{sat} = 1.2e-4$  [m/s] and  $\alpha = 0.174$  [1/kPa]).

#### 3.5.2 | Effect of saturated hydraulic conductivity

Similar to the dynamic coefficient, saturated hydraulic conductivity was changed by one order of magnitude compared to the value of ISS0-sand (Level 2). As revealed by Figure 21, the effect of saturated hydraulic conductivity was more pronounced on the value of the normalized difference in shear strength and did not significantly affect the time to mechanical equilibrium. A 10-fold change in the value of saturated hydraulic conductivity resulted in a 15% change in the normalized difference in maximum shear stress (from 25% for Level 2 to 10% and above 35% for Levels 1 and 3, respectively).

#### 3.5.3 | Effect of air entry value

As shown in Figure 22, similar to the effect of saturated conductivity, the change in the van Genuchten  $\alpha$ -parameter, or air entry value, mainly influenced the normalized difference in maximum shear stress. About 1 kPa change in the air entry

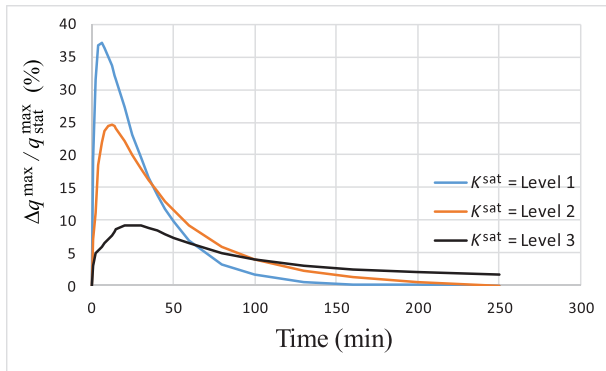


**FIGURE 21** The results of the parametric study: The effect of saturated hydraulic conductivity on the normalized difference in the maximum shear stress ( $\alpha = 0.174$  [1/kPa] and  $\tau = 5.25e6 - 0.379e6 S_w$  [Pa·s]).

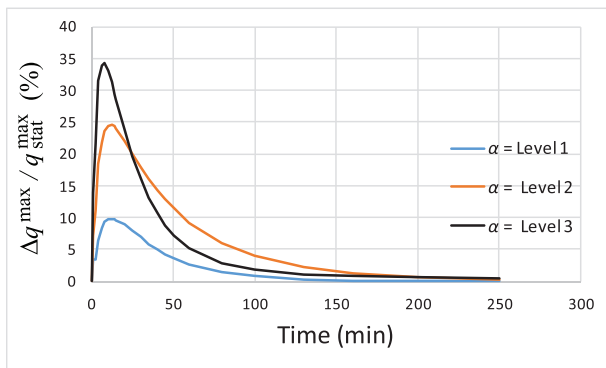


**FIGURE 22** The results of the parametric study: The effect of air entry values on the normalized difference in the maximum shear stress ( $K^{sat} = 1.2e-4$  [m/s] and  $\tau = 5.25e6 - 0.379e6 S_w$  [Pa·s]).

value of the ISS0-sand, corresponding to the considered values of  $\alpha$  (0.148, 0.174, and 0.211), altered the normalized difference in maximum shear stress from about 25% (Level 2) to 10% and 35% for Levels 1 and 3, respectively. Therefore, the dynamic coefficient had the highest impact among the three studied parameters. However, the effect of saturated conductivity and the air entry value on hydro-mechanical response should not be overlooked.

## 4 | CONCLUSION

This study presented simulations of triaxial tests conducted on a sandy soil subjected to transient unsaturated flow. The shearing of soil at different times was simulated, and resulting shear stress–strain curves were analyzed and compared. The flow simulations were conducted considering two modeling scenarios with and without the inclusion of the dynamic capillarity effects. Furthermore, various boundary conditions that ranged from low to high pressure and flowrate values

were considered. A sensitivity study was also carried out on the effect of three hydraulic parameters. The findings are as follows:

- Verification of the flow model against a benchmark transient flow experiment indicates that the dynamic scenario can capture the observed experimental behavior much better than the static scenario.
- A higher value of boundary conditions (flowrate or pressure) results in a more pronounced difference between the static and dynamic flow results.
- In the simulations with flowrate boundary conditions, the temporal evolution of  $P^{diff}$  (the difference in phase pressures) obtained using the dynamic formulation is considerably higher than that of the static simulation scenario (with a difference of up to 72%).
- In the simulations with pressure boundary conditions, the temporal evolution of sample saturation obtained through the dynamic formulation shows higher values than the one obtained from the static case, with the difference reaching up to 61%, depending on the imposed pressure. Furthermore, the change of  $P^{diff}$  with time is nonmonotonic, following a similar trend observed in the previous experimental studies.
- The soil shear strength during drainage, analyzed with dynamic capillarity formulation and subjected to triaxial loading, is found to be up to 150% of the static shear strength, depending on the magnitude of boundary condition values, proving the importance of the dynamic capillarity effect.
- The significance of dynamic capillary effects on the mechanical response of soil is influenced by the confining pressure and reduces as the confinement increases. This highlights the potential significance of dynamic capillarity effects in shallow rainfall-induced landslides or near-surface failures induced by rapid fill-up or drawdown in dams and embankments.
- The parametric study indicates the much higher influence of the dynamic coefficient compared to saturated conductivity and air entry value. Besides, the dynamic coefficient affects the time to mechanical equilibration. Higher values of dynamic coefficient correspond to longer mechanical equilibrium time.

Based on the findings of this research, the following suggestions can be highlighted for future studies:

- While the drainage process simulated in this study can be a proxy for a large-scale phenomenon, such as the rapid drawdown of an earth dam, a more critical situation would be a rainfall-induced landslide or a rapid fill-up of an earth dam, in which the imbibition process is dominant. Although, based on Equation (4) and the findings of this study, one

can expect lower shear strength for the sample during the wetting process, it needs more in-depth analyses to unravel its magnitude and other complexities.

- Hysteresis effects can also be taken into consideration to add more accuracy to simulations, particularly in the case of multiple drainage and imbibition cycles such as antecedent rainfalls where the soil has experienced multiple events of rainfall.
- In this study, a one-way coupled model was used to investigate the effects of dynamic capillarity on the peak shear strength of the samples. One step forward would be a fully coupled model to shed light on the samples' post-failure and critical state behavior subjected to transient two-phase flow.

## AUTHOR CONTRIBUTIONS

**Alireza Daman Shokouh:** Conceptualization; formal analysis; investigation; methodology; software; validation; writing—original draft; writing—review and editing. **Ehsan Nikooee:** Conceptualization; formal analysis; methodology; project administration; supervision; writing—original draft; writing—review and editing. **Ghassem Habibagahi:** Conceptualization; formal analysis; methodology; project administration; supervision; writing—review and editing. **S. Majid Hassanizadeh:** Conceptualization; formal analysis; methodology; supervision; writing—review and editing.

## ACKNOWLEDGMENTS

The authors would like to express their sincere gratitude to Professor Guido Musso, as well as Dr. Luwen Zhuang, Dr. Marius Milatz, and Dr. Amir Hossein Tavangarrad for the fruitful discussions throughout this study. Furthermore, SMH acknowledges support by the Stuttgart Center for Simulation Science (SimTech).

## CONFLICT OF INTEREST STATEMENT

The authors declare no conflicts of interest.

## ORCID

Alireza Daman Shokouh  <https://orcid.org/0009-0006-6776-0719>

Ehsan Nikooee  <https://orcid.org/0000-0003-2365-1132>

## REFERENCES

- Bishop, A. W. (1959). The principal of effective stress. *Teknisk ukeblad*, 39, 859–863.
- Bottero, S., Hassanizadeh, S. M., Kleingeld, P. J., & Heimovaara, T. J. (2011). Nonequilibrium capillarity effects in two-phase flow through porous media at different scales. *Water Resources Research*, 47(10), W10505. <https://doi.org/10.1029/2011WR010887>
- Brooks, R. H., & Corey, A. T. (1966). Properties of porous media affecting fluid flow. *Journal of the Irrigation and Drainage Division*, 92(2), 61–88. <https://doi.org/10.1061/JRCEA4.0000425>
- Camps-Roach, G., O'Carroll, D. M., Newson, T. A., Sakaki, T., & Illangasekare, T. H. (2010). Experimental investigation of dynamic effects in capillary pressure: Grain size dependency and upscaling. *Water Resources Research*, 46(8), W08544. <https://doi.org/10.1029/2009WR008881>
- Chen, Y., Mao, Y., Yang, L., Wei, W., Meng, Q., & Cai, J. (2022). A comprehensive review of factors affecting dynamic capillary effect in two-phase flow. *Transport in Porous Media*, 144(1), 33–54. <https://doi.org/10.1007/s11242-021-01723-x>
- Cosentini, R. M., Della Vecchia, G., Foti, S., & Musso, G. (2012). Estimation of the hydraulic parameters of unsaturated samples by electrical resistivity tomography. *Géotechnique*, 62(7), 583–594. <https://doi.org/10.1680/geot.10.P.066>
- Davis, R. O., & Selvadurai, A. P. (2005). *Plasticity and geomechanics*. Cambridge University Press.
- Diamantopoulos, E., & Durner, W. (2012). Dynamic nonequilibrium of water flow in porous media: A review. *Vadose Zone Journal*, 11(3), vzj2011.0197. <https://doi.org/10.2136/vzj2011.0197>
- Fazli Ghiyasabadi, S., Habibagahi, G., & Nikooee, E. (2021). A capillary water-retention framework for the effective stress parameter considering hydraulic hysteresis. *Transport in Porous Media*, 138(3), 489–509. <https://doi.org/10.1007/s11242-021-01626-x>
- Goel, G., & O'Carroll, D. M. (2011). Experimental investigation of nonequilibrium capillarity effects: Fluid viscosity effects. *Water Resources Research*, 47(9), W09507. <https://doi.org/10.1029/2010WR009861>
- Griffiths, D., & Lu, N. (2005). Unsaturated slope stability analysis with steady infiltration or evaporation using elasto-plastic finite elements. *International Journal for Numerical and Analytical Methods in Geomechanics*, 29(3), 249–267. <https://doi.org/10.1002/nag.413>
- Guo, H., Cheng, L., Jia, P., & Cao, R. (2023). An improved method for fitting relative permeability curve using nuclear magnetic resonance imaging. *Geoenergy Science and Engineering*, 227, 211812. <https://doi.org/10.1016/j.geoen.2023.211812>
- Hassanizadeh, S. M., Celia, M. A., & Dahle, H. K. (2002). Dynamic effect in the capillary pressure—Saturation relationship and its impacts on unsaturated flow. *Vadose Zone Journal*, 1(1), 38–57. <https://doi.org/10.2136/vzj2002.3800>
- Hassanizadeh, S. M., & Gray, W. G. (1990). Mechanics and thermodynamics of multiphase flow in porous media including interphase boundaries. *Advances in Water Resources*, 13(4), 169–186. [https://doi.org/10.1016/0309-1708\(90\)90040-B](https://doi.org/10.1016/0309-1708(90)90040-B)
- Hassanizadeh, S. M., & Gray, W. G. (1993). Thermodynamic basis of capillary pressure in porous media. *Water Resources Research*, 29(10), 3389–3405. <https://doi.org/10.1029/93WR01495>
- Huyghe, J., Nikooee, E., & Hassanizadeh, S. (2017). Bridging effective stress and soil water retention equations in deforming unsaturated porous media: A thermodynamic approach. *Transport in Porous Media*, 117(3), 349–365. <https://doi.org/10.1007/s11242-017-0837-9>
- Khalili, N., Geiser, F., & Blight, G. (2004). Effective stress in unsaturated soils: Review with new evidence. *International Journal of Geomechanics*, 4(2), 115–126. [https://doi.org/10.1061/\(ASCE\)1532-3641\(2004\)4:2\(115\)](https://doi.org/10.1061/(ASCE)1532-3641(2004)4:2(115))
- Khalili, N., Romero, E., & Marinho, F. A. (2022). State of the Art Report. Advances in Unsaturated Soil Mechanics: Constitutive modelling, experimental investigation, and field instrumentation. In *Proceedings of Twentieth International Conference on Soil Mechanics and Geotechnical Engineering (ICSMGE 2022)*. (pp. 297–348) International Society for Soil Mechanics and Geotechnical Engineering.
- Li, Y., Liu, C., Li, H., Chen, S., Lu, K., Zhang, Q., & Luo, H. (2022). A review on measurement of the dynamic effect in capillary pressure.

- Journal of Petroleum Science and Engineering*, 208, 109672. <https://doi.org/10.1016/j.petrol.2021.109672>
- Lu, N., Khalili, N., Nikoee, E., & Hassanizadeh, S. M. (2014). Principle of effective stress in variably saturated porous media. *Vadose Zone Journal*, 13(5), 1–4. <https://doi.org/10.2136/vzj2014.04.0038>
- Mantney, S., Hassanizadeh, S. M., & Helmig, R. (2005). Macro-scale dynamic effects in homogeneous and heterogeneous porous media. In D. B. Das & S. M. Hassanizadeh (Eds.), *Upscaling multiphase flow in porous media* (pp. 121–145). Springer.
- Milatz, M., Törzs, T., Nikoee, E., Hassanizadeh, S. M., & Grabe, J. (2018). Theoretical and experimental investigations on the role of transient effects in the water retention behaviour of unsaturated granular soils. *Geomechanics for Energy and the Environment*, 15, 54–64. <https://doi.org/10.1016/j.gete.2018.02.003>
- Mirzaei, M., & Das, D. B. (2007). Dynamic effects in capillary pressure—Saturations relationships for two-phase flow in 3D porous media: Implications of micro-heterogeneities. *Chemical Engineering Science*, 62(7), 1927–1947. <https://doi.org/10.1016/j.ces.2006.12.039>
- Mirzaei, M., & Das, D. B. (2013). Experimental investigation of hysteretic dynamic effect in capillary pressure—Saturation relationship for two-phase flow in porous media. *AIChE Journal*, 59(10), 3958–3974. <https://doi.org/10.1002/aic.14121>
- Moeckel, G. P. (1975). Thermodynamics of an interface. *Archive for Rational Mechanics and Analysis*, 57(3), 255–280. <https://doi.org/10.1007/BF00280158>
- Nikoee, E., Habibagahi, G., Hassanizadeh, S. M., & Ghahramani, A. (2012). The effective stress in unsaturated soils: Insights from thermodynamics. In C. Mancuso, C. Jummi, & F. D’Onza (Eds.), *Unsaturated soils: Research and applications* (Vol 2, pp. 5–11). Springer.
- Nikoee, E., Habibagahi, G., Hassanizadeh, S. M., & Ghahramani, A. (2013). Effective stress in unsaturated soils: A thermodynamic approach based on the interfacial energy and hydromechanical coupling. *Transport in Porous Media*, 96, 369–396. <https://doi.org/10.1007/s11242-012-0093-y>
- Nikoee, E., Hassanizadeh, S. M., & Habibagahi, G. (2013). Mechanics of unsaturated soils: From equilibrium to transient conditions. *Poromechanics V: Proceedings of the Fifth Biot Conference on Poromechanics*.
- O’Carroll, D. M., Phelan, T. J., & Abriola, L. M. (2005). Exploring dynamic effects in capillary pressure in multistep outflow experiments. *Water Resources Research*, 41(11), W11419. <https://doi.org/10.1029/2005WR004010>
- Pryor, R. W. (2009). *Multiphysics modeling using COMSOL: A first principles approach*. Jones & Bartlett Publishers.
- Sakaki, T., O’Carroll, D. M., & Illangasekare, T. H. (2010). Direct quantification of dynamic effects in capillary pressure for drainage–wetting cycles. *Vadose Zone Journal*, 9(2), 424–437. <https://doi.org/10.2136/vzj2009.0105>
- Sheng, P., & Zhou, M. (1992). Immiscible-fluid displacement: Contact-line dynamics and the velocity-dependent capillary pressure. *Physical Review A*, 45(8), 5694. <https://doi.org/10.1103/PhysRevA.45.5694>
- Topp, G., Klute, A., & Peters, D. (1967). Comparison of water content–pressure head data obtained by equilibrium, steady-state, and unsteady-state methods. *Soil Science Society of America Journal*, 31(3), 312–314. <https://doi.org/10.2136/sssaj1967.03615995003100030009x>
- van Genuchten, M. Th. (1980). A closed-form equation for predicting the hydraulic conductivity of unsaturated soils. *Soil Science Society of America Journal*, 44(5), 892–898. <https://doi.org/10.2136/sssaj1980.03615995004400050002x>
- Yan, G., Bore, T., Schlaeger, S., Scheuermann, A., & Li, L. (2024). Dynamic effects in soil water retention curves: an experimental exploration by full-scale soil column tests using spatial time-domain reflectometry and tensiometers. *Acta Geotechnica*. <https://doi.org/10.1007/s11440-024-02328-6>
- Yan, G., Li, Z., Galindo Torres, S. A., Scheuermann, A., & Li, L. (2022). Transient two-phase flow in porous media: A literature review and engineering application in geotechnics. *Geotechnics*, 2(1), 32–90. <https://doi.org/10.3390/geotechnics2010003>
- Zhuang, L., Hassanizadeh, S. M., Qin, C. Z., & de Waal, A. (2017). Experimental investigation of hysteretic dynamic capillarity effect in unsaturated flow. *Water Resources Research*, 53(11), 9078–9088. <https://doi.org/10.1002/2017WR020895>

**How to cite this article:** Daman Shokouh, A., Nikoee, E., Habibagahi, G., & Hassanizadeh, S. M. (2024). Effects of dynamic capillarity on the shear strength of sandy soils during transient two-phase flow: Insights from non-equilibrium triaxial simulations. *Vadose Zone Journal*, 23, e20351. <https://doi.org/10.1002/vzj2.20351>